PHYSICAL REVIEW B **96**, 201305(R) (2017)

Nodal-knot semimetals

Ren Bi,[1] Zhongbo Yan,[1] Ling Lu,[2] and Zhong Wang[1,3,*]

[1]*Institute for Advanced Study, Tsinghua University, Beijing 100084, China*

[2]*Institute of Physics, Chinese Academy of Sciences, Beijing National Laboratory for Condensed Matter Physics, Beijing 100190, China*

[3]*Collaborative Innovation Center of Quantum Matter, Beijing 100871, China*

(Received 23 April 2017; revised manuscript received 3 August 2017; published 20 November 2017)

Topological nodal-line semimetals are characterized by one-dimensional lines of band crossing in the Brillouin zone. In contrast to nodal points, nodal lines can be in topologically nontrivial configurations. In this Rapid Communication, we introduce the concept of "nodal-knot semimetals," whose nodal lines form topologically nontrivial knots in the Brillouin zone. We introduce a generic construction of nodal-knot semimetals, which yields the simplest trefoil nodal knot and other more complicated nodal knots. The knotted-unknotted transitions by nodal-line reconnections are also studied. Our work brings the knot theory to the subject of topological semimetals.

DOI: 10.1103/PhysRevB.96.201305

Introduction. Topological states have been under intense investigations in the last decade [1–5]. Topological semimetals [6] are characterized by topologically protected nodal points or nodal lines in the Brillouin zone, where the valence band and conduction band meet each other. The most extensively studied nodal-point semimetals are Weyl semimetals [7–28] and Dirac semimetals [29–37]. More recently, nodal-line semimetals have attracted considerable attention. Like the Dirac points, nodal lines [38–54] are protected by both the band topology and symmetries. Nodal-line semimetals are versatile platforms for topological materials. By breaking certain symmetry, nodal lines can be partially or fully gapped, giving way to Dirac semimetals, Weyl semimetals, or topological insulators. These phenomena can be triggered by the spin-orbit coupling [46,47] or external driving [55–61]. There are quite a few material candidates of nodal lines: ZrSiS [62,63], calcium phosphide [64,65], carbon networks [44], CaP_3 [66], alkaline-earth-metal materials [67,68], magnon nodal lines in Cu_3TeO_6 [69], to name a few. Experimental studies of nodal lines are also in rapid progress [45,62,63,70–73].

Nodal points have little internal structure, e.g., the only topological characterization of a Weyl point is its chirality (± 1). In contrast, nodal lines have much richer topologically distinct possibilities. They can touch each other and form nodal chains stretching across the Brillouin zone [74–76] [Fig. 1(b)]. Another intriguing possibility is the nodal link [77–79], namely, two nodal lines topologically linked with each other [Fig. 1(c)]. Links are also proposed in superconductors [80].

Nodal links are not the simplest topologically nontrivial shapes of nodal lines. The simplest shape contains only one nodal line entangled with itself, i.e., a knot. We emphasize that a nominal nodal link can sometimes be trivial because the two linked rings may come from independent bands [81]; in contrast, a nodal knot must be nontrivial. An example is the trefoil nodal knot, shown in Fig. 1(d). A crucial question is whether such a conception can exist in principle (i.e., can be explicitly constructed as models). The recently proposed method of constructing nodal links based on Hopf mappings cannot be applied to yield a nodal knot, because it necessarily produces multiple nodal lines [78]. It is thus unclear whether a single-line nodal knot is realizable in materials. Here, we introduce a method based on functions of several complex variables, which neatly gives various single-line nodal knots, including the trefoil knot as the simplest case. The topological transitions from the knotted configurations to trivial ones are also studied. Our work brings the extensively investigated knot theory [82] to the subject of topological semimetals.

Continuum models. Nodal lines stem from the crossing of two adjacent bands, thus we focus on two-band models below. Any two-band model can be written as

$$H(\mathbf{k}) = a_1(\mathbf{k})\sigma_x + a_2(\mathbf{k})\sigma_y + a_3(\mathbf{k})\sigma_z + a_0(\mathbf{k})\mathbf{1}, \qquad (1)$$

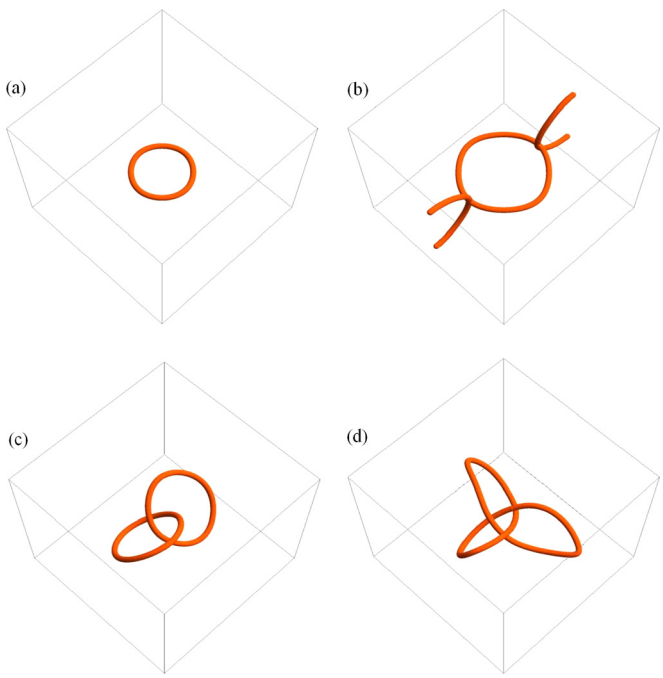

FIG. 1. Schematic illustration of four types of nodal line: (a) ordinary nodal ring, (b) nodal chain, (c) nodal link, and (d) nodal knot. A nodal knot is a single nodal line entangled with itself.

*wangzhongemail@gmail.com

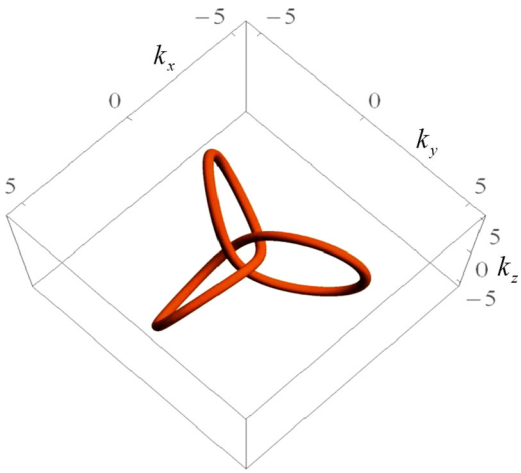

FIG. 2. The trefoil nodal knot of the continuum model in Eq. (10). The parameter m in Eq. (10) is $m = 0.5$.

where σ_i's are the Pauli matrices, and the trivial $a_0(\mathbf{k})$ term will be discarded below. Nodal lines are protected by the cooperation of band topology and certain symmetries [83–85]. In this work, we consider the combination of spatial-inversion symmetry $\mathcal{P}$ and time-reversal symmetry $\mathcal{T}$ [47,50,86], which is quite common in materials. The $\mathcal{PT}$ symmetry ensures that $H^*(\mathbf{k}) = H(\mathbf{k})$ up to a basis choice [50], thus we have $a_2(\mathbf{k}) = 0$. Given the symmetry, the Hamiltonian becomes

$$H(\mathbf{k}) = a_1(\mathbf{k})\sigma_x + a_3(\mathbf{k})\sigma_z, \tag{2}$$

whose energies are $E_\pm(\mathbf{k}) = \pm\sqrt{a_1^2(\mathbf{k}) + a_3^2(\mathbf{k})}$, and the nodal lines can be solved from $a_1(\mathbf{k}) = a_3(\mathbf{k}) = 0$. The most common choices of a_1 and a_3, say $a_1 = \cos k_x + \cos k_y + \cos k_z - m_0, a_3 = \sin k_z$, yield ordinary nodal lines resembling Fig. 1(a). Taking advantage of the Hopf mappings [87–95], nodal links such as the one shown in Fig. 1(c) can be constructed [78]. This method is general enough to generate nodal links with any integer linking numbers (including the simplest Hopf link), however, it is unable to generate a single-line nodal knot.

In this Rapid Communication, we introduce a generic approach for constructing nodal knots, which is based on functions of several complex variables. Let us start from the geometrical preparations. Let us consider two complex variables z and w, with the constraint $|z|^2 + |w|^2 = 1$, which defines a 3-sphere. This is more transparent if we write $z = n_1 + in_2$ and $w = n_3 + in_4$, then $|z|^2 + |w|^2 = 1$ becomes $n_1^2 + n_2^2 + n_3^2 + n_4^2 = 1$, which is apparently a 3-sphere. For reasons to become clear shortly, let us consider the surface $|z|^p = |w|^q$ (where p,q are positive integers) in the 3-sphere. This surface is topologically a 2-torus. To see this fact, we notice that the two equations $|z|^2 + |w|^2 = 1$ and $|z|^p = |w|^q$ completely fix the values of $|z|$ and $|w|$, thus the surface can be parametrized by the phases θ_z and θ_w, which are defined in $z = |z|\exp(i\theta_z)$ and $w = |w|\exp(i\theta_w)$, respectively. Thus the surface is exactly a 2-torus, with θ_z and θ_w parametrizing the toroidal and poloidal direction, respectively.

Now we impose a constraint

$$f(z,w) \equiv z^p + w^q = 0. \tag{3}$$

The solutions (z,w) of this constraint must be on the torus $|z|^p = |w|^q$ discussed above; furthermore, the phases have to satisfy $p\theta_z - q\theta_w = \pi \pmod{2\pi}$. As a mathematical fact of torus geometry, when p and q are relatively prime, the equation defines only one line on the torus. Otherwise, we have multiple lines. For instance, when $(p,q) = (3,2)$, we have a single line passing the point $(\theta_z,\theta_w) = (\pi/3,0)$; when $(p,q) = (2,4)$, we have two disconnected lines, one of which passes $(\theta_z,\theta_w) = (\pi/2,0)$ and the other passes $(\theta_z,\theta_w) = (\pi/2,\pi/2)$. Most notably, when both p and q are nonzero, the line(s) winds around the torus in both the toroidal and poloidal directions, forming a knot when (p,q) are relatively prime, or links otherwise.

With these geometrical preparations, we are now ready to construct continuum models of nodal-knot semimetals. For continuum models, the momentum variables $\mathbf{k} = (k_x,k_y,k_z)$ extend to infinity. In the above construction of knot, the standard 3-sphere $n_1^2 + n_2^2 + n_3^2 + n_4^2 = 1$ is considered. To make use of this construction, we can compactify the $\mathbf{k}$ space to a 3-sphere by adding an "infinity point." (This is a standard procedure in topology, which is essentially the converse of stereographic projection.) We may establish a one-to-one correspondence between the compactified $\mathbf{k}$ space and the standard 3-sphere. There are infinitely many ways to do this; for instance, we can take

$$N_1 = k_x, \quad N_2 = k_y, \quad N_3 = k_z, \quad N_4 = m - k^2/2, \tag{4}$$

with $k^2 = k_x^2 + k_y^2 + k_z^2$ and $m > 0$, and define $n_i = N_i/N$ with $N = \sqrt{N_1^2 + N_2^2 + N_3^2 + N_4^2}$. Now $\mathbf{n}(\mathbf{k}) = (n_1,n_2,n_3,n_4)$ maps the compactified $\mathbf{k}$ space to the standard 3-sphere. It maps the origin $\mathbf{k} = (0,0,0)$ to the north pole $\mathbf{n} = (0,0,0,1)$, and the $\mathbf{k}$ infinity to the south pole $\mathbf{n} = (0,0,0,-1)$. The winding number of the mapping is known as

$$W = \frac{1}{2\pi^2}\int dk_x dk_y dk_z\, \epsilon^{abcd} n_a \partial_{k_x} n_b \partial_{k_y} n_c \partial_{k_z} n_d, \tag{5}$$

which is found to be -1 here. This is intuitively clear since the 3-sphere is covered only once. In fact, any other mapping with a nonzero winding number is applicable for our construction.

Now that $z = n_1 + in_2$ and $w = n_3 + in_4$ have become functions of $\mathbf{k}$, we can take the coefficients a_1 and a_3 in Eq. (2) as functions of z and w. A natural choice is the real part and imaginary part of $f(z,w)$, respectively:

$$a_1(\mathbf{k}) = \mathrm{Re}\, f(z,w), \quad a_3(\mathbf{k}) = \mathrm{Im}\, f(z,w). \tag{6}$$

Equations (3) and (6) are among the key equations of this Rapid Communication. With this ansatz, the nodal line equation $a_1(\mathbf{k}) = a_3(\mathbf{k}) = 0$ is simply $f(z,w) = 0$, i.e., Eq. (3), which gives rise to a knot when (p,q) are relatively prime, as explained above. This is the motivation of the ansatz. To simplify, we can take

$$z = N_1 + iN_2, \quad w = N_3 + iN_4 \tag{7}$$

in Eq. (6), which is topologically equivalent to taking $z = n_1 + in_2$, $w = n_3 + in_4$, because $\mathbf{n}(\mathbf{k})$ and $\mathbf{N}(\mathbf{k})$ differ only

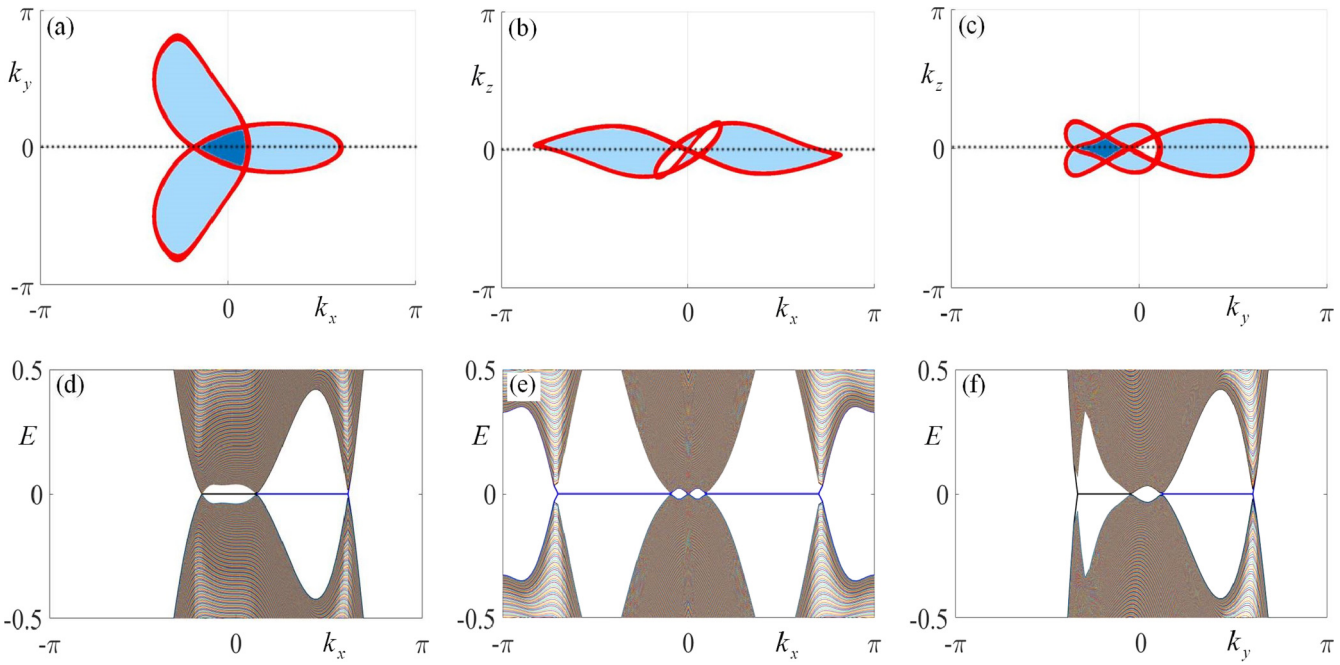

FIG. 3. (a)–(c) Nodal knots projected to the surface Brillouin zone (red lines), and the regions of surface bands (light-blue regions have one band, while dark-blue regions have two bands). (d)–(f) The surface-state energy dispersions plotted along the dashed lines in (a)–(c), respectively. The Bloch Hamiltonian is Eq. (11) with $m_0 = 2.8$.

by a numerical factor $N(\mathbf{k})$. Hereafter we take the convention of Eq. (7).

In the case $(p,q) = (3,2)$, we have

$$f(z,w) = (N_1 + iN_2)^3 + (N_3 + iN_4)^2, \tag{8}$$

and the ansatz in Eq. (6) leads to

$$\begin{aligned} a_1(\mathbf{k}) &= N_1^3 - 3N_1N_2^2 + N_3^2 - N_4^2, \\ a_3(\mathbf{k}) &= 3N_1^2N_2 - N_2^3 + 2N_3N_4, \end{aligned} \tag{9}$$

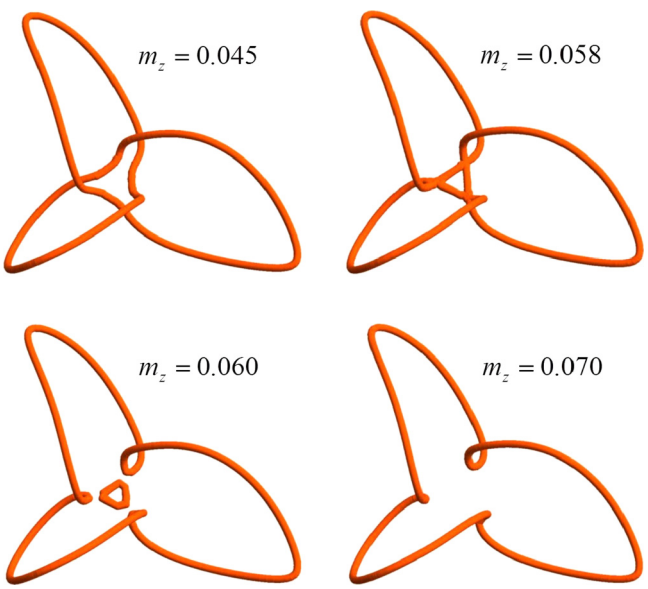

FIG. 4. The evolution of nodal knot as a function of m_z. Here, $m_0 = 2.8$ is fixed.

thus the Bloch Hamiltonian reads

$$\begin{aligned} H(\mathbf{k}) = &\left[k_x^3 - 3k_xk_y^2 + k_z^2 - (m - k^2/2)^2\right]\sigma_x \\ &+ \left[3k_x^2k_y - k_y^3 + 2k_z(m - k^2/2)\right]\sigma_z. \end{aligned} \tag{10}$$

The nodal line of this model is shown in Fig. 2, which is apparently a trefoil nodal knot. Many other nodal knots can be obtained in this way by taking other (p,q) or $\mathbf{N}(\mathbf{k})$ functions.

Lattice models and knotted-unknotted transitions. For lattice models, the $\mathbf{k}$ space (Brillouin zone) is a 3-torus T^3. One may generalize the method of the previous section, replacing the $\mathbf{N}(\mathbf{k})$ function by a periodic one. (This construction is given in the Supplemental Material [96]). Here, we introduce another scheme. We construct Bloch Hamiltonians whose expansions near certain points (say $\mathbf{k} = 0$) resemble the continuum models of nodal knots such as Eq. (10). As an example, we take on a cubic lattice

$$\begin{aligned} H_l(\mathbf{k}) = \sigma_x &\left[\sin k_x(1 - \cos k_x) - 3\sin k_x(1 - \cos k_y) + \sin^2 k_z \right. \\ &\left. - \left(\sum_i \cos k_i - m_0\right)^2\right] + \sigma_z\left[3\sin k_y(1 - \cos k_x)\right. \\ &\left. - \sin k_y(1 - \cos k_y) + 2\sin k_z\left(\sum_i \cos k_i - m_0\right)\right]. \end{aligned} \tag{11}$$

The hopping range is quite short in this model (to the second nearest neighbor). The nodal knot of this model with $m_0 = 2.8$ has been shown in Fig. 1(d) as a representative of nodal knots. The surface states for open boundary systems are shown in

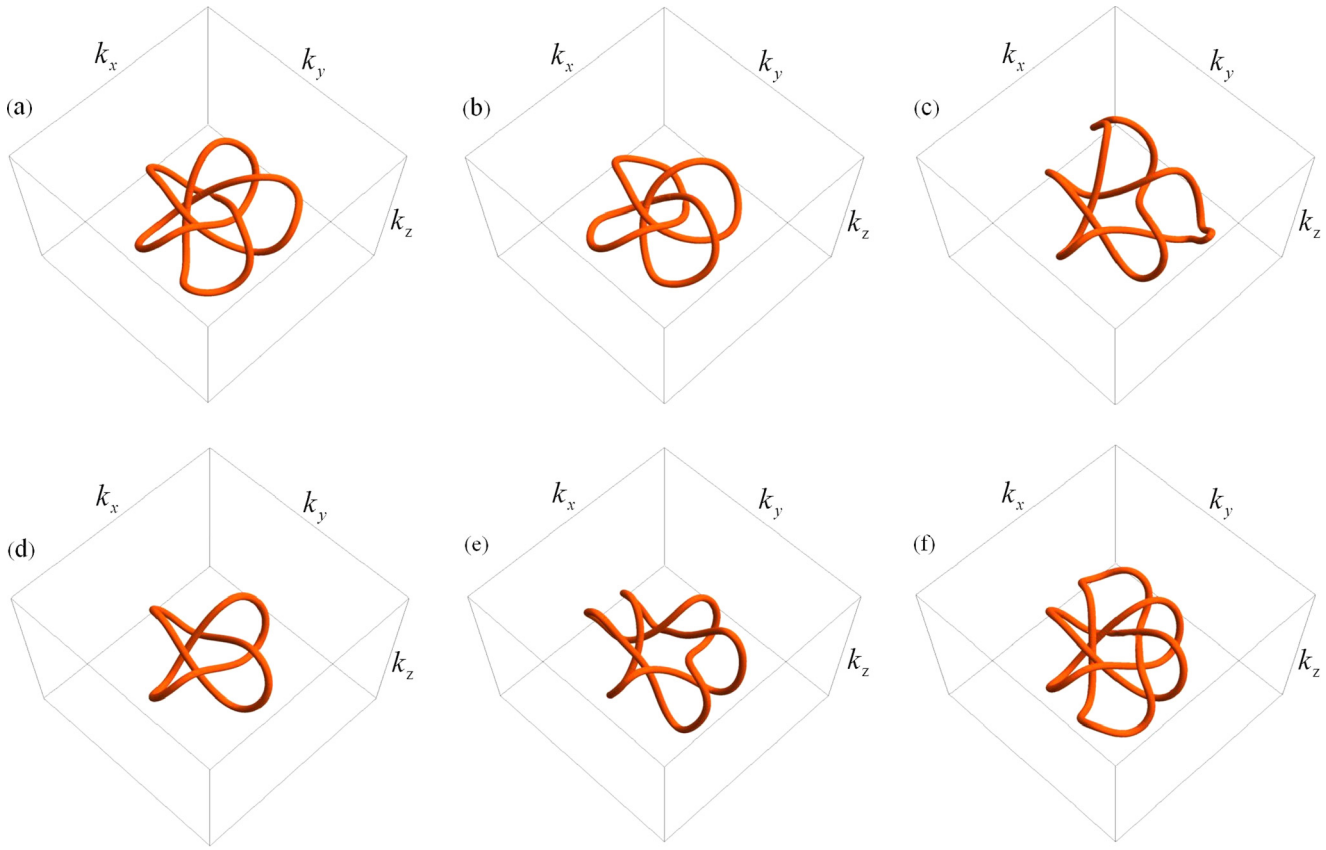

FIG. 5. Nodal knots and nodal links for several values of (p,q). The Hamiltonian is given by the ansatz Eq. (6); $m_0 = 2.5$. (a) $(p,q) = (5,3)$; (b) $(p,q) = (4,3)$; (c) $(p,q) = (5,2)$; (d) $(p,q) = (4,2)$; (e) $(p,q) = (6,2)$; (f) $(p,q) = (6,3)$. In (a)–(c) we have a nodal knot (a single knotted nodal line), while in (d)–(f) we have a nodal link. In the cases (a)–(c), p and q are relatively prime; in (d)–(f), they are not.

Fig. 3. The **k**-space boundary of the surface-state bands is the nodal knot projected to the surface Brillouin zone. As the Hamiltonian has a chiral symmetry (the σ_y term is absent), the number of surface zero-energy bands is determined by the winding number [97] in each region of the surface Brillouin zone.

This method is applicable to many other crystal symmetries (see Supplemental Material for a model with threefold rotational symmetry). So far, we have focused on $\mathcal{PT}$ symmetry; if both $\mathcal{P}$ and $\mathcal{T}$ are present, one can obtain a single $\mathcal{P}$-symmetric nodal knot, or two nodal knots, one of them being the image of the other under $\mathcal{P}$ operation (see Supplemental Material [96]).

It is also interesting to investigate the transition from the unknotted nodal lines to the knotted ones. To this end, we add an additional $m_z\sigma_z$ term into the Bloch Hamiltonian of Eq. (11), namely, we consider $H_l'(\mathbf{k}) = H_l(\mathbf{k}) + m_z\sigma_z$. The evolution of the nodal knot of H_l' as a function of m_z is shown in Fig. 4. As we increase m_z, the nodal knot gradually deforms. Around $m_z \approx 0.058$, there are three successive (very close to each other) nodal-line reconnection transitions, taking place at three different locations in the Brillouin zone. At the reconnection transition, two pieces of nodal line come close to each other, touch, and then separate with the lines reconnected. After the reconnections, the original nodal knot evolves to two nodal rings [Fig. 4(c)]. As we further increase m_z, the smaller ring shrinks and finally disappears. At $m_z = 0.07$, we have a single unknotted nodal line [Fig. 4(d)].

We have focused on the simplest case $(p,q) = (3,2)$ for simplicity. In fact, the method is general and applicable to all other pairs of integers. As we have explained, nodal knots can be obtained when (p,q) are relatively prime, otherwise nodal links are obtained. We have shown the nodal knots and nodal links for several choices of (p,q) in Fig. 5 [98]. In Figs. 5(a)–5(c), different shapes of nodal knots can be found. In contrast, Figs. 5(d)–5(f) are nodal links due to the fact that the pairs of integers (4,2), (6,2), and (6,3) are not relatively prime. The even smaller nonrelatively prime integers (2,2) gives a nodal link similar to Fig. 1(c).

Conclusions. Knots are often studied in the real space. Here, we have introduced nodal knots in the momentum space (Brillouin zone) in the context of topological semimetals [99,100], which leads to the concept of nodal-knot semimetals. We hope that this work can stimulate the search of realistic materials. It will also be interesting to study possible topological terms and topological responses of nodal-knot semimetals, which may have interesting observable consequences in electromagnetic properties and thermal transports [101]. On the theoretical side, further applications of the knot theory [82] to topological matters may be rewarding.

Note added. Recently, we became aware of a related work [102]. Although nodal knots are also discussed there, their method, as a generalization of Ref. [78], can only generate nodal links. Their nominal "trefoil knot" is constructed at the

price of introducing an unavoidable discontinuity (a branch cut) in the Bloch Hamiltonian.

Acknowledgments. R.B., Z.Y., and Z.W. are supported by NSFC (Grants No. 11674189 and No. 11304175). Z.Y. is supported in part by China Postdoctoral Science Foundation (2016M590082). L.L is supported by the National key R&D Program of China (Grants No. 2017YFA0303800 and No. 2016YFA0302400) and NSFC under Project No. 11721404.

R.B. and Z.Y. contributed equally to this work.

[1] M. Z. Hasan and C. L. Kane, "*Colloquium*: Topological insulators," Rev. Mod. Phys. **82**, 3045 (2010).

[2] X.-L. Qi and S.-C. Zhang, Topological insulators and superconductors, Rev. Mod. Phys. **83**, 1057 (2011).

[3] A. Bansil, H. Lin, and T. Das, "*Colloquium*: Topological band theory," Rev. Mod. Phys. **88**, 021004 (2016).

[4] B. A. Bernevig and T. L. Hughes, *Topological Insulators and Topological Superconductors* (Princeton University Press, Princeton, NJ, 2013).

[5] S.-Q. Shen, *Topological Insulators: Dirac Equation in Condensed Matters* (Springer-verlag, Berlin, Heidelberg, 2012), Vol. 174.

[6] C.-K. Chiu, J. C. Y. Teo, A. P. Schnyder, and S. Ryu, Classification of topological quantum matter with symmetries, Rev. Mod. Phys. **88**, 035005 (2016).

[7] X. Wan, A. M. Turner, A. Vishwanath, and S. Y. Savrasov, Topological semimetal and Fermi-arc surface states in the electronic structure of pyrochlore iridates, Phys. Rev. B **83**, 205101 (2011).

[8] S. Murakami, Phase transition between the quantum spin Hall and insulator phases in 3D: Emergence of a topological gapless phase, New J. Phys. **9**, 356 (2007).

[9] S. Murakami and S.-i. Kuga, Universal phase diagrams for the quantum spin Hall systems, Phys. Rev. B **78**, 165313 (2008).

[10] A. A. Burkov and L. Balents, Weyl Semimetal in a Topological Insulator Multilayer, Phys. Rev. Lett. **107**, 127205 (2011).

[11] K.-Y. Yang, Y.-M. Lu, and Y. Ran, Quantum Hall effects in a Weyl semimetal: Possible application in pyrochlore iridates, Phys. Rev. B **84**, 075129 (2011).

[12] G. E. Volovik, *The Universe in a Helium Droplet* (Oxford University Press, New York, 2003).

[13] H. Weng, C. Fang, Z. Fang, B. A. Bernevig, and X. Dai, Weyl Semimetal Phase in Noncentrosymmetric Transition-Metal Monophosphides, Phys. Rev. X **5**, 011029 (2015).

[14] S.-M. Huang, S.-Y. Xu, I. Belopolski, C.-C. Lee, G. Chang, B. Wang, N. Alidoust, G. Bian, M. Neupane, A. Bansil, H. Lin, and M. Z. Hasan, An inversion breaking Weyl semimetal state in the TaAs material class, Nat. Commun. **6**, 7373 (2015).

[15] S.-Y. Xu, I. Belopolski, N. Alidoust, M. Neupane, G. Bian, C. Zhang, R. Sankar, G. Chang, Z. Yuan, C.-C. Lee *et al.*, Discovery of a Weyl fermion semimetal and topological Fermi arcs, Science **349**, 613 (2015).

[16] B. Q. Lv, H. M. Weng, B. B. Fu, X. P. Wang, H. Miao, J. Ma, P. Richard, X. C. Huang, L. X. Zhao, G. F. Chen *et al.*, Experimental Discovery of Weyl Semimetal TaAs, Phys. Rev. X **5**, 031013 (2015).

[17] X. Huang, L. Zhao, Y. Long, P. Wang, D. Chen, Z. Yang, H. Liang, M. Xue, H. Weng, Z. Fang, X. Dai, and G. Chen, Observation of the Chiral-Anomaly-Induced Negative Magnetoresistance in 3D Weyl Semimetal TaAs, Phys. Rev. X **5**, 031023 (2015).

[18] S.-Y. Xu, N. Alidoust, I. Belopolski, C. Zhang, G. Bian, T.-R. Chang, H. Zheng, V. Strokov, D. S. Sanchez, G. Chang, Z. Yuan, D. Mou, Y. Wu, L. Huang, C.-C. Lee, S.-M. Huang, B. Wang, A. Bansil, H.-T. Jeng, T. Neupert, A. Kaminski, H. Lin, S. Jia, and M. Z. Hasan, Discovery of Weyl semimetal NbAs, Nat. Phys. **11**, 748 (2015).

[19] L. X. Yang, Z. K. Liu, Y. Sun, H. Peng, H. F. Yang, T. Zhang, B. Zhou, Y. Zhang, Y. F. Guo, M. Rahn *et al.*, Weyl semimetal phase in the non-centrosymmetric compound TaAs, Nat. Phys. **11**, 728 (2015).

[20] C. Shekhar, A. K Nayak, Y. Sun, M. Schmidt, M. Nicklas, I. Leermakers, U. Zeitler, Y. Skourski, J. Wosnitza, Z. Liu *et al.*, Extremely large magnetoresistance and ultrahigh mobility in the topological Weyl semimetal candidate NbP, Nat. Phys. **11**, 645 (2015).

[21] L. Lu, Z. Wang, D. Ye, L. Ran, L. Fu, J. D. Joannopoulos, and M. Soljačić, Experimental observation of Weyl points, Science **349**, 622 (2015).

[22] R. Bi and Z. Wang, Unidirectional transport in electronic and photonic Weyl materials by Dirac mass engineering, Phys. Rev. B **92**, 241109 (2015).

[23] A. A. Soluyanov, D. Gresch, Z. Wang, Q. Wu, M. Troyer, X. Dai, and B. A. Bernevig, Type-II Weyl semimetals, Nature (London) **527**, 495 (2015).

[24] Y. Sun, S.-C. Wu, M. N. Ali, C. Felser, and B. Yan, Prediction of Weyl semimetal in orthorhombic $MoTe_2$, Phys. Rev. B **92**, 161107 (2015).

[25] T.-R. Chang, S.-Y. Xu, G. Chang, C.-C. Lee, S.-M. Huang, B. Wang, G. Bian, H. Zheng, D. S Sanchez, I. Belopolski *et al.*, Prediction of an arc-tunable Weyl fermion metallic state in $Mo_xW_{1-x}Te_2$, Nat. Commun. **7**, 10639 (2016).

[26] X.-Q. Sun, S.-C. Zhang, and Z. Wang, Helical Spin Order from Topological Dirac and Weyl Semimetals, Phys. Rev. Lett. **115**, 076802 (2015).

[27] A. A. Zyuzin and A. A. Burkov, Topological response in Weyl semimetals and the chiral anomaly, Phys. Rev. B **86**, 115133 (2012).

[28] Z. Wang and S.-C. Zhang, Chiral anomaly, charge density waves, and axion strings from Weyl semimetals, Phys. Rev. B **87**, 161107 (2013).

[29] M. Neupane, S.-Y. Xu, R. Sankar, N. Alidoust, G. Bian, C. Liu, I. Belopolski, T.-R. Chang, H.-T. Jeng, H. Lin, A. Bansil, F. Chou, and M. Z. Hasan, Observation of a three-dimensional topological Dirac semimetal phase in high-mobility Cd_3As_2, Nat. Commun. **5**, 3786 (2014).

[30] S.-Y. Xu, C. Liu, S. K Kushwaha, R. Sankar, J. W. Krizan, I. Belopolski, M. Neupane, G. Bian, N. Alidoust, T.-R. Chang *et al.*, Observation of Fermi arc surface states in a topological metal, Science **347**, 294 (2015).

[31] Z. K. Liu, B. Zhou, Y. Zhang, Z. J. Wang, H. M. Weng, D. Prabhakaran, S.-K. Mo, Z. X. Shen, Z. Fang, X. Dai *et al.*,

Discovery of a three-dimensional topological Dirac semimetal, Na_3Bi, Science **343**, 864 (2014).

[32] S. Borisenko, Q. Gibson, D. Evtushinsky, V. Zabolotnyy, B. Büchner, and R. J. Cava, Experimental Realization of a Three-Dimensional Dirac Semimetal, Phys. Rev. Lett. **113**, 027603 (2014).

[33] S. M. Young, S. Zaheer, J. C. Y. Teo, C. L. Kane, E. J. Mele, and A. M. Rappe, Dirac Semimetal in Three Dimensions, Phys. Rev. Lett. **108**, 140405 (2012).

[34] Z. Wang, Y. Sun, X.-Q. Chen, C. Franchini, G. Xu, H. Weng, X. Dai, and Z. Fang, Dirac semimetal and topological phase transitions in A_3Bi (A = Na, K, Rb), Phys. Rev. B **85**, 195320 (2012).

[35] Z. Wang, H. Weng, Q. Wu, X. Dai, and Z. Fang, Three-dimensional Dirac semimetal and quantum transport in Cd_3As_2, Phys. Rev. B **88**, 125427 (2013).

[36] R. Y. Chen, Z. G. Chen, X.-Y. Song, J. A. Schneeloch, G. D. Gu, F. Wang, and N. L. Wang, Magnetoinfrared Spectroscopy of Landau Levels and Zeeman Splitting of Three-Dimensional Massless Dirac Fermions in $ZrTe_5$, Phys. Rev. Lett. **115**, 176404 (2015).

[37] Y. Liu, X. Yuan, C. Zhang, Z. Jin, A. Narayan, C. Luo, Z. Chen, L. Yang, J. Zou, X. Wu *et al.*, Zeeman splitting and dynamical mass generation in Dirac semimetal $ZrTe_5$, Nat. Commun. **7**, 12516 (2016).

[38] A. A. Burkov, M. D. Hook, and L. Balents, Topological nodal semimetals, Phys. Rev. B **84**, 235126 (2011).

[39] M. Phillips and V. Aji, Tunable line node semimetals, Phys. Rev. B **90**, 115111 (2014).

[40] J.-M. Carter, V. V. Shankar, M. A. Zeb, and H.-Y. Kee, Semimetal and topological insulator in perovskite iridates, Phys. Rev. B **85**, 115105 (2012).

[41] C.-K. Chiu and A. P. Schnyder, Classification of reflection-symmetry-protected topological semimetals and nodal superconductors, Phys. Rev. B **90**, 205136 (2014).

[42] M. Zeng, C. Fang, G. Chang, Y.-A. Chen, T. Hsieh, A. Bansil, H. Lin, and L. Fu, Topological semimetals and topological insulators in rare earth monopnictides, arXiv:1504.03492.

[43] Y. Chen, Y.-M. Lu, and H.-Y. Kee, Topological crystalline metal in orthorhombic perovskite iridates, Nat. Commun. **6**, 6593 (2015).

[44] H. Weng, Y. Liang, Q. Xu, R. Yu, Z. Fang, X. Dai, and Y. Kawazoe, Topological node-line semimetal in three-dimensional graphene networks, Phys. Rev. B **92**, 045108 (2015).

[45] G. Bian, T.-R. Chang, R. Sankar, S.-Y. Xu, H. Zheng, T. Neupert, C.-K. Chiu, S.-M. Huang, G. Chang, I. Belopolski, D. S. Sanchez, M. Neupane, N. Alidoust, C. Liu, B. Wang, C.-C. Lee, H.-T. Jeng, A. Bansil, F. Chou, H. Lin, and M. Z. Hasan, Topological nodal-line fermions in spin-orbit metal $PbTaSe_2$, Nat. Commun. **7**, 10556 (2016).

[46] R. Yu, H. Weng, Z. Fang, X. Dai, and X. Hu, Topological Node-Line Semimetal and Dirac Semimetal State in Antiperovskite Cu_3PdN, Phys. Rev. Lett. **115**, 036807 (2015).

[47] Y. Kim, B. J. Wieder, C. L. Kane, and A. M. Rappe, Dirac Line Nodes in Inversion-Symmetric Crystals, Phys. Rev. Lett. **115**, 036806 (2015).

[48] J.-W. Rhim and Y. B. Kim, Landau level quantization and almost flat modes in three-dimensional semimetals with nodal ring spectra, Phys. Rev. B **92**, 045126 (2015).

[49] Y. Chen, Y. Xie, S. A. Yang, H. Pan, F. Zhang, M. L. Cohen, and S. Zhang, Spin-orbit-free Weyl-loop and Weyl-point semimetals in a stable three-dimensional carbon allotrope, Nano Lett. **15**, 6974 (2015).

[50] C. Fang, Y. Chen, H.-Y. Kee, and L. Fu, Topological nodal line semimetals with and without spin-orbital coupling, Phys. Rev. B **92**, 081201 (2015).

[51] K. Mullen, B. Uchoa, and D. T. Glatzhofer, Line of Dirac Nodes in Hyperhoneycomb Lattices, Phys. Rev. Lett. **115**, 026403 (2015).

[52] G. Bian, T.-R. Chang, H. Zheng, S. Velury, S.-Y. Xu, T. Neupert, C.-K. Chiu, S.-M. Huang, D. S. Sanchez, I. Belopolski, N. Alidoust, P.-J. Chen, G. Chang, A. Bansil, H.-T. Jeng, H. Lin, and M. Z. Hasan, Drumhead surface states and topological nodal-line fermions in $TlTaSe_2$, Phys. Rev. B **93**, 121113 (2016).

[53] R. Yu, Z. Fang, X. Dai, and H. Weng, Topological nodal line semimetals predicted from first-principles calculations, Front. Phys. **12**, 127202 (2017).

[54] Z. Yan, P.-W. Huang, and Z. Wang, Collective modes in nodal line semimetals, Phys. Rev. B **93**, 085138 (2016).

[55] Z. Yan and Z. Wang, Tunable Weyl Points in Periodically Driven Nodal Line Semimetals, Phys. Rev. Lett. **117**, 087402 (2016).

[56] C.-K. Chan, Y.-T. Oh, J. H. Han, and P. A. Lee, Type-II Weyl cone transitions in driven semimetals, Phys. Rev. B **94**, 121106 (2016).

[57] A. Narayan, Tunable point nodes from line-node semimetals via application of light, Phys. Rev. B **94**, 041409 (2016).

[58] X.-X. Zhang, T. T. Ong, and N. Nagaosa, Theory of photoinduced Floquet Weyl semimetal phases, Phys. Rev. B **94**, 235137 (2016).

[59] K. Taguchi, D.-H. Xu, A. Yamakage, and K. T. Law, Photovoltaic anomalous Hall effect in line-node semimetals, Phys. Rev. B **94**, 155206 (2016).

[60] M. Ezawa, Photoinduced topological phase transition from a crossing-line nodal semimetal to a multiple-Weyl semimetal, Phys. Rev. B **96**, 041205 (2017).

[61] Z. Yan and Z. Wang, Floquet multi-Weyl points in crossing-nodal-line semimetals, Phys. Rev. B **96**, 041206 (2017).

[62] L. M. Schoop, M. N Ali, C. Straßer, V. Duppel, S. S. P. Parkin, B. V. Lotsch, and C. R. Ast, Dirac cone protected by non-symmorphic symmetry and 3D Dirac line node in ZrSiS, Nat. Commun. **7**, 11696 (2016).

[63] M. Neupane, I. Belopolski, M. M. Hosen, D. S. Sanchez, R. Sankar, M. Szlawska, S.-Y. Xu, K. Dimitri, N. Dhakal, P. Maldonado, P. M. Oppeneer, D. Kaczorowski, F. Chou, M. Z. Hasan, and T. Durakiewicz, Observation of topological nodal fermion semimetal phase in ZrSiS, Phys. Rev. B **93**, 201104 (2016).

[64] Y.-H. Chan, C.-K. Chiu, M. Y. Chou, and A. P. Schnyder, Ca_3P_2 and other topological semimetals with line nodes and drumhead surface states, Phys. Rev. B **93**, 205132 (2016).

[65] L. S. Xie, L. M. Schoop, E. M. Seibel, Q. D. Gibson, W. Xie, and R. J. Cava, A new form of Ca_3P_2 with a ring of Dirac nodes, APL Mater. **3**, 083602 (2015).

[66] Q. Xu, R. Yu, Z. Fang, X. Dai, and H. Weng, Topological nodal line semimetals in the CaP_3 family of materials, Phys. Rev. B **95**, 045136 (2017).

[67] R. Li, H. Ma, X. Cheng, S. Wang, D. Li, Z. Zhang, Y. Li, and X.-Q. Chen, Dirac Node Lines in Pure Alkali Earth Metals, Phys. Rev. Lett. **117**, 096401 (2016).

[68] M. Hirayama, R. Okugawa, T. Miyake, and S. Murakami, Topological Dirac nodal lines and surface charges in fcc alkaline earth metals, Nat. Commun. **8**, 14022 (2017).

[69] K. Li, C. Li, J. Hu, Y. Li, and C. Fang, Dirac and Nodal-Line Magnons in Collinear Antiferromagnets, Phys. Rev. Lett. (to be published).

[70] J. Hu, Z. Tang, J. Liu, X. Liu, Y. Zhu, D. Graf, Y. Shi, S. Che, C. N. Lau, J. Wei *et al.*, Topological Nodal-Line Fermions in ZrSiSe and ZrSiTe, Phys. Rev. Lett. **117**, 016602 (2016).

[71] R. Singha, A. Pariari, B. Satpati, and P. Mandal, Large non-saturating magnetoresistance and signature of nondegenerate Dirac nodes in ZrSiS, Proc. Natl. Acad. Sci. USA **114**, 2468 (2017).

[72] X. Wang, X. Pan, M. Gao, J. Yu, J. Jiang, J. Zhang, H. Zuo, M. Zhang, Z. Wei, W. Niu, Z. Xia, X. Wan, Y. Chen, F. Song, Y. Xu, B. Wang, G. Wang, and R. Zhang, Evidence of both surface and bulk Dirac bands in ZrSiS and the unconventional magnetoresistance, Adv. Electron. Mater. **2**, 1600228 (2016).

[73] C. Chen, X. Xu, J. Jiang, S.-C. Wu, . P. Qi, L. X. Yang, M. X. Wang, Y. Sun, N. B. M. Schröter, H. F. Yang *et al.*, Dirac line nodes and effect of spin-orbit coupling in the nonsymmorphic critical semimetals MSiS (M = Hf, Zr), Phys. Rev. B **95**, 125126 (2017).

[74] T. Bzdušek, Q. Wu, A. Rüegg, M. Sigrist, and A. A. Soluyanov, Nodal-chain metals, Nature (London) **538**, 75 (2016).

[75] R. Yu, Q. Wu, Z. Fang, and H. Weng, From Nodal Chain Semimetal To Weyl Semimetal in HfC, Phys. Rev. Lett. **119**, 036401 (2017).

[76] Q. Yan, R. Liu, Z. Yan, B. Liu, H. Chen, Z. Wang, and L. Lu, Experimental discovery of nodal chains, arXiv:1706.05500.

[77] W. Chen, H.-Z. Lu, and J.-M. Hou, Topological semimetals with a double-helix nodal link, Phys. Rev. B **96**, 041102 (2017).

[78] Z. Yan, R. Bi, H. Shen, L. Lu, S.-C. Zhang, and Z. Wang, Nodal-link semimetals, Phys. Rev. B **96**, 041103 (2017).

[79] P.-Y. Chang and C.-H. Yee, Weyl-link semimetals, Phys. Rev. B **96**, 081114 (2017).

[80] X.-Q. Sun, B. Lian, and S.-C. Zhang, Double Helix Nodal Line Superconductor, Phys. Rev. Lett. **119**, 147001 (2017).

[81] The nodal links in Refs. [77,78] are nontrivial because the nodal rings come from the same two bands.

[82] L. H. Kauffman, *Knots and Physics* (World Scientific, Singapore, 2001), Vol. 1.

[83] P. Hořava, Stability of Fermi Surfaces and k Theory, Phys. Rev. Lett. **95**, 016405 (2005).

[84] Y. X. Zhao and Z. D. Wang, Topological Classification and Stability of Fermi Surfaces, Phys. Rev. Lett. **110**, 240404 (2013).

[85] Y. X. Zhao, A. P. Schnyder, and Z. D. Wang, Unified Theory of Pt and CP Invariant Topological Metals and Nodal Superconductors, Phys. Rev. Lett. **116**, 156402 (2016).

[86] Y. X. Zhao and Y. Lu, PT-Symmetric Real Dirac Fermions and Semimetals, Phys. Rev. Lett. **118**, 056401 (2017).

[87] F. Wilczek and A. Zee, Linking Numbers, Spin, and Statistics of Solitons, Phys. Rev. Lett. **51**, 2250 (1983).

[88] J. E. Moore, Y. Ran, and X.-G. Wen, Topological Surface States in Three-Dimensional Magnetic Insulators, Phys. Rev. Lett. **101**, 186805 (2008).

[89] D.-L. Deng, S.-T. Wang, C. Shen, and L.-M. Duan, Hopf insulators and their topologically protected surface states, Phys. Rev. B **88**, 201105 (2013).

[90] D.-L. Deng, S.-T. Wang, K. Sun, and L.-M. Duan, Probe knots and Hopf insulators with ultracold atoms, arXiv:1612.01518.

[91] D.-L. Deng, S.-T. Wang, and L.-M. Duan, Systematic construction of tight-binding Hamiltonians for topological insulators and superconductors, Phys. Rev. B **89**, 075126 (2014).

[92] R. Kennedy, Topological Hopf-Chern insulators and the Hopf superconductor, Phys. Rev. B **94**, 035137 (2016).

[93] C. Wang, P. Zhang, X. Chen, J. Yu, and H. Zhai, Measuring Topological Number of a Chern-Insulator from Quench Dynamics, Phys. Rev. Lett. **118**, 185701 (2017).

[94] C. Liu, F. Vafa, and C. Xu, Symmetry-protected topological Hopf insulator and its generalizations, Phys. Rev. B **95**, 161116 (2017).

[95] Z. Yan, R. Bi, and Z. Wang, Majorana Zero Modes Protected by a Hopf Invariant in Topologically Trivial Superconductors, Phys. Rev. Lett. **118**, 147003 (2017).

[96] See Supplemental Material at http://link.aps.org/supplemental/10.1103/PhysRevB.96.201305 for (i) a different scheme of constructing lattice models; (ii) Model with threefold rotational symmetry; (iii) Model with P and T symmetries.

[97] S. Ryu and Y. Hatsugai, Topological Origin of Zero-Energy Edge States in Particle-Hole Symmetric Systems, Phys. Rev. Lett. **89**, 077002 (2002).

[98] Here, we have taken $N_1 = \sin k_x, N_2 = \sin k_y, N_3 = \sin k_z$, $N_4 = \sum_{i=x,y,z} \cos k_i - m_0$.

[99] N. P. Armitage, E. J. Mele, and A. Vishwanath, Weyl and Dirac semimetals in three dimensional solids, arXiv:1705.01111 (2017).

[100] C. Fang, H. Weng, X. Dai, and Z. Fang, Topological nodal line semimetals, Chin. Phys. B **25**, 117106 (2016).

[101] B. Lian, C. Vafa, F. Vafa, and S.-C. Zhang, Chern-Simons theory and Wilson loops in the Brillouin zone, Phys. Rev. B **95**, 094512 (2017).

[102] M. Ezawa, Topological semimetals carrying arbitrary Hopf numbers: Hopf-link, Solomon's-knot, trefoil-knot, and other semimetals, Phys. Rev. B **96**, 041202(R) (2017).

Supplemental Material of "Nodal-knot semimetals"

Ren Bi[†],[1] Zhongbo Yan[†],[1] Ling Lu,[2] and Zhong Wang[1,3,*]

[1]*Institute for Advanced Study, Tsinghua University, Beijing, 100084, China*
[2]*Institute of Physics, Chinese Academy of Sciences/Beijing National Laboratory for Condensed Matter Physics, Beijing 100190, China*
[3]*Collaborative Innovation Center of Quantum Matter, Beijing, 100871, China*

A DIFFERENT SCHEME OF CONSTRUCTING LATTICE MODELS OF NODAL KNOT

In the main article, we have constructed lattice models of nodal knot by first constructing continuum models of nodal knots, then writing down Bloch Hamiltonians whose expansion near certian points (such as $\mathbf{k} = 0$) resemble the continuum models. In the section, we present another construction.

For lattice models, the $\mathbf{k}$-space (Brillouin zone) is a 3-torus T^3. The main difference compared to the continuum model is that $\mathbf{N}(\mathbf{k})$ must be periodic in $\mathbf{k}$, otherwise the construction is similar. Following the lead of Eq.(4) in the main article, we can choose

$$N_1 = \sin k_x, \quad N_2 = \sin k_y, \quad N_3 = \sin k_z,$$
$$N_4 = \sum_{i=x,y,z} \cos k_i - m_0. \tag{1}$$

Expanding N_4 in Eq.(1) to the first order, we can see that $3-m_0$ plays the role of m. Now Eq.(6) in the main article gives rise to models of nodal knots in lattice models. According to Eq.(6) in the main article, the Bloch Hamiltonian for the simplest case $(p, q) = (3, 2)$ is given by Eq.(2) in the main article with

$$a_1(\mathbf{k}) = \sin^2 k_z - (\sum_i \cos k_i - m_0)^2 + \sin^3 k_x - 3 \sin k_x \sin^2 k_y,$$
$$a_3(\mathbf{k}) = 2 \sin k_z (\sum_i \cos k_i - m_0) + 3 \sin^2 k_x \sin k_y - \sin^3 k_y. \tag{2}$$

It hosts a nodal knot for $1 < m_0 < 3$ (in this regime, the previously defined winding number $W = -1$). The nodal knot of $m_0 = 2.5$ is shown in Fig.1.

It is also interesting to investigate the transition from the unknotted nodal lines to the knotted ones. To this end, we add an additional $m_z\sigma_z$ term into the Bloch Hamiltonian:

$$a_1 = \sin^2 k_z - (\sum_i \cos k_i - m_0)^2 + \sin^3 k_x - 3 \sin k_x \sin^2 k_y,$$
$$a_3 = 2 \sin k_z (\sum_i \cos k_i - m_0) + 3 \sin^2 k_x \sin k_y - \sin^3 k_y + m_z. \tag{3}$$

The evolution of nodal knot as a function of m_z is shown in Fig.2. As we increase m_z, the nodal knot gradually deforms. Around $m_z \approx 0.13$, there are three successive (very close to each other) nodal-line reconnection transitions, taking place at three different locations in the Brillouin zone. At the reconnection transition, two pieces of nodal line come close to each other, touch, and then separate with the lines reconnected. After the reconnections, the original nodal knot evolves to two nodal rings [Fig.2(c)]. As we further increase m_z, the smaller ring shrinks and finally disappears. At $m_z = 0.14$, we have a single unknotted nodal line [Fig.2(d)].

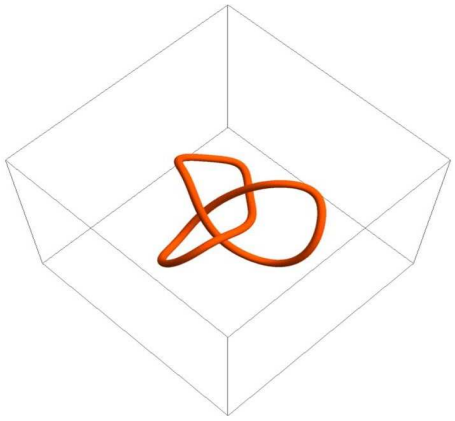

FIG. 1. The nodal knot for the lattice model in Eq.(2), with $m_0 = 2.5$.

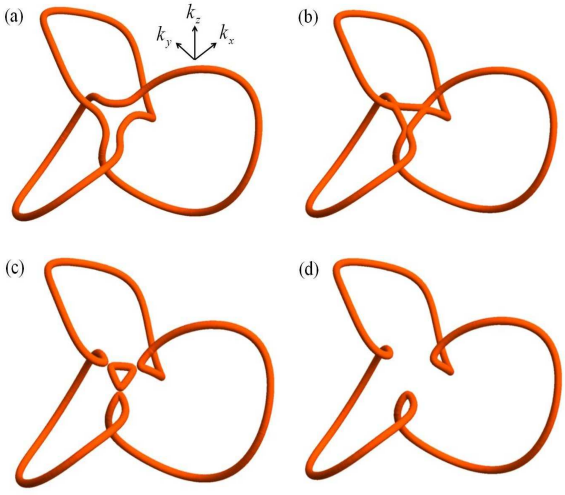

FIG. 2. The evolution of nodal knot as a function of m_z. Here, $m_0 = 2.7$ is fixed. (a) $m_z = 0.1200$; knotted. (b) $m_z = 0.1316$; critical. (c) $m_z = 0.1335$; unknotted (two rings). (d) $m_z = 0.1400$; unknotted (single ring).

NODAL-KNOT SEMIMETAL WITH THREEFOLD ROTATIONAL SYMMETRY

In the main article, we have studied models of nodal knots in the cubic lattice, nevertheless, the scheme of construction

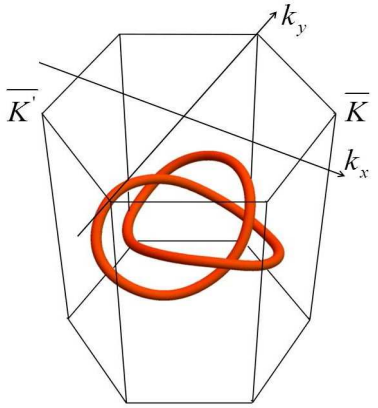

FIG. 3. Nodal knot for $m_0 = 2.8$. $\bar{\mathbf{K}} = (\frac{2\pi}{3}, \frac{2\pi}{3\sqrt{3}})$ and $\bar{\mathbf{K}}' = -(\frac{2\pi}{3}, \frac{2\pi}{3\sqrt{3}})$ are high symmetric points in the Brillouin zone. The model and the nodal knot have threefold rotational symmetry.

is general. In this section, we apply it to a lattice with threefold rotational symmetry, a simple hexagonal Bravais lattice. Inspired by the continuum model, we find that the following Bloch Hamiltonian hosts a trefoil nodal knot:

$$\begin{aligned} H(\mathbf{k}) = [&(\sin k_x - 2\sin\frac{k_x}{2}\cos\frac{\sqrt{3}k_y}{2}) + \sin^2 k_z \\ &-(\cos k_x + 2\cos\frac{k_x}{2}\cos\frac{\sqrt{3}k_y}{2} + \cos k_z - m_0)^2]\sigma_x \\ &+[2\sin k_z(\cos k_x + 2\cos\frac{k_x}{2}\cos\frac{\sqrt{3}k_y}{2} + \cos k_z - m_0) \\ &+(\sin\sqrt{3}k_y - 2\sin\frac{\sqrt{3}k_y}{2}\cos\frac{3k_x}{2})]\sigma_z, \end{aligned} \tag{4}$$

or equivalently,

$$\begin{aligned} H(\mathbf{k}) = [&(\sin k_x - 2\sin\frac{k_x}{2}\cos\frac{\sqrt{3}k_y}{2}) - \cos 2k_z \\ &+(2m_0 - 1 - 2\cos k_z)(\cos k_x + 2\cos\frac{k_x}{2}\cos\frac{\sqrt{3}k_y}{2}) \\ &-(\cos 2k_x + 2\cos k_x\cos\sqrt{3}k_y) - m_0^2 - \frac{3}{2} \\ &-(\cos\sqrt{3}k_y + 2\cos\frac{3k_x}{2}\cos\frac{\sqrt{3}k_y}{2})]\sigma_x \\ &+[2\sin k_z(\cos k_x + 2\cos\frac{k_x}{2}\cos\frac{\sqrt{3}k_y}{2}) + \sin 2k_z \\ &-2m_0\sin k_z + (\sin\sqrt{3}k_y - 2\sin\frac{\sqrt{3}k_y}{2}\cos\frac{3k_x}{2})]\sigma_z. \end{aligned}$$

Besides the threefold rotational symmetry, this Bloch Hamiltonian has three reflection axes, which are $k_y = k_z = 0$; $k_y = \sqrt{3}k_x$, $k_z = 0$; and $k_y = -\sqrt{3}k_x$, $k_z = 0$, which can be expressed as $R_1 H(k_x, k_y, k_z)R_1^{-1} = H(k_x, -k_y, -k_z)$, $R_2 H(k_x, k_y, k_z)R_2^{-1} = H(-\frac{k_x}{2} + \frac{\sqrt{3}k_y}{2}, \frac{\sqrt{3}k_x}{2} + \frac{k_y}{2}, -k_z)$, $R_3 H(k_x, k_y, k_z)R_3^{-1} = H(-\frac{k_x}{2} - \frac{\sqrt{3}k_y}{2}, -\frac{\sqrt{3}k_x}{2} + \frac{k_y}{2}, -k_z)$, with $R_{i=1,2,3} = \sigma_x$.

The nodal knot for $m_0 = 2.8$ is shown in Fig.3.

NODAL KNOTS WITH BOTH $\mathcal{P}$ AND $\mathcal{T}$ SYMMETRIES

In the main article, we have considered a model with $\mathcal{PT}$ symmetry, but no $\mathcal{P}$ or $\mathcal{T}$ separately. Here, we provide a model with both $\mathcal{P}$ and $\mathcal{T}$ symmetries. Again, we follow the scheme of constructing Bloch Hamiltonians whose expansion near certain points resemble the continuum models of nodal knots. Inspired by the continuum model in the main article, we put forward the following Bloch Hamiltonian

$$\begin{aligned} H(\mathbf{k}) = [&\lambda_1(\cos^3 k_x - 3\cos k_x\cos^2 k_y) + \lambda_2\cos^2 k_z - \lambda_3(\sum_i \cos 2k_i - m_0)^2]\tau_x \\ &+[\lambda_4\cos k_z(\sum_i \cos 2k_i - m_0) + \lambda_5(3\cos^2 k_x\cos k_y - \cos^3 k_y)]\tau_z. \end{aligned} \tag{5}$$

which has time-reversal symmetry, inversion symmetry, mirror-reflection symmetry, and C_2 rotation symmetry. It hosts eight trefoil knots near $\mathbf{Q}_i = (\pm\pi/2, \pm\pi/2, \pm\pi/2)$, re-

spectively. A $\mathcal{P}$-symmetric Hamiltonian with less nodal knots can be obtained as

$$H(\mathbf{k}) = [\lambda_1(\cos^3 k_x - 6\cos k_x(1-\cos k_y)) + \lambda_2 \sin^2 k_z - \lambda_3(\cos k_y + \cos k_z - \gamma\cos 2k_x - m_0)^2]\tau_x$$
$$+[\lambda_4 \sin k_z(\cos k_y + \cos k_z - \gamma\cos 2k_x - m_0) + \lambda_5(3\cos^2 k_x \sin k_y - 2\sin k_y(1-\cos k_y))]\tau_z. \quad (6)$$

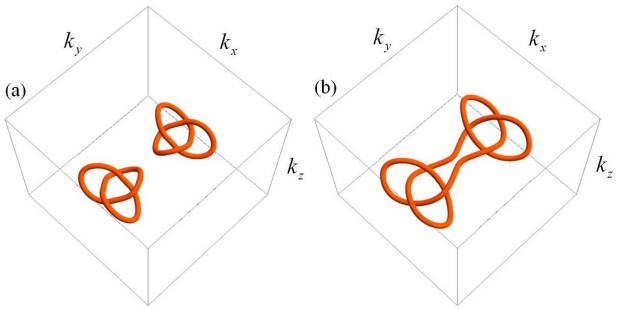

FIG. 4. Nodal knots of the Bloch Hamiltonian in Eq.(6). $\lambda_1 = \lambda_5 = 0.2$, $\lambda_2 = \lambda_3 = 1$, $\lambda_4 = 2$, $\gamma = 0.4$. (a) $m_0 = 2.1$. (b) $m_0 = 2.0$. The first Brillouin zone $k_x \times k_y \times k_z \in [-\pi, \pi] \times [-\pi, \pi] \times [-\pi, \pi]$ is shown.

This Hamiltonian is also inspired by the continuum model of nodal knot. When the Hamiltonian is expanded near $K_\pm = \pm(\pi/2, 0, 0)$, the resultant continuum Hamiltonian is just the one given in the main article. This Hamiltonian has $\mathcal{P}$ symmetry, i.e., $\mathcal{P}H(\mathbf{k})\mathcal{P}^{-1} = H(-\mathbf{k})$ with $\mathcal{P} = \tau_x$, time-reversal symmetry, i.e., $\mathcal{T}H(\mathbf{k})\mathcal{T}^{-1} = H^*(-\mathbf{k})$ with $\mathcal{T} = \tau_x\mathcal{K}$ ($\mathcal{K}$ denotes the complex conjugation).

The nodal knots of Eq.(6) is shown in Fig.4 for two values of m_0. Interestingly, a topological Lifshitz transition takes place as m_0 is tuned, causing the combination of two trefoil nodal knots to a single knot.

* wangzhongemail@tsinghua.edu.cn
†These two authors contribute equally to this work.